

# Advanced Vadose Zone Simulations Using TOUGH

*S. Finsterle\*, C. Doughty, M.B. Kowalsky,*

*G.J. Moridis, L. Pan, T. Xu, Y. Zhang, and K. Pruess*

Lawrence Berkeley National Laboratory

Earth Sciences Division

1 Cyclotron Road, Mail Stop 90-1116

Berkeley, CA 94720, U.S.A.

e-mail: SAFinsterle@lbl.gov

## ABSTRACT

The vadose zone can be characterized as a complex subsurface system in which intricate physical and biogeochemical processes occur in response to a variety of natural forcings and human activities. This makes it difficult to describe, understand, and predict the behavior of this specific subsurface system. The TOUGH nonisothermal multiphase flow simulators are well-suited to perform advanced vadose zone studies. The conceptual models underlying the TOUGH simulators are capable of representing features specific to the vadose zone, and of addressing a variety of coupled phenomena. Moreover, the simulators are integrated into software tools that enable advanced data analysis, optimization, and system-level modeling. We discuss fundamental and computational challenges in simulating vadose zone processes, review recent advances in modeling such systems, and demonstrate some capabilities of the TOUGH suite of codes using illustrative examples.

## 22 INTRODUCTION

23 Water flow through variably saturated porous media is commonly described by the  
24 Richards equation (Richards, 1931). The Richards equation exhibits strong nonlinearities,  
25 which calls for numerical solution methods whenever the model is applied to realistic  
26 systems. The TOUGH suite of numerical simulators for nonisothermal flows of  
27 multiphase, multicomponent fluids in permeable (fractured and porous) media (Pruess et  
28 al., 1999; Pruess, 2004a) is based on conceptualizations and methodologies that are well  
29 suited for the solution of vadose zone flow and transport problems. Moreover, the  
30 emphasis of TOUGH on an accurate description of hydrogeological features, physical  
31 processes, and thermodynamic properties makes it a useful tool for studying and  
32 predicting more complex phenomena occurring near the land surface or in deeper  
33 unsaturated zones, either using the classical Richards equation or employing more  
34 complex, nonisothermal multiphase flow and reactive transport processes. Table 1 shows  
35 a summary of the main TOUGH codes.

36 In this review article, we discuss some of the modeling issues specific to the  
37 simulation of vadose zone processes, and present examples of recent developments of the  
38 TOUGH suite of codes aimed at addressing some of these issues. Table 2 summarizes the  
39 simulation capabilities and applications presented in this paper along with key references.

## 40 VADOSE ZONE MODELING CHALLENGES

41 Traditionally, soil physicists and agronomists perform vadose zone modeling studies  
42 that focus on the prediction of moisture, soil-gas, and heat flow as well as nutrient and  
43 pesticide transport in the shallow, variably saturated crop root zone. In addition to these

44 traditional applications, the scope of numerical simulations in the unsaturated zone has  
45 been considerably broadened both in terms of systems and processes considered. The  
46 depth and horizontal scale of vadose zone systems studied by numerical models has been  
47 greatly expanded, and may include deep unsaturated zones that are affected by  
48 contamination, considered for storage of carbon dioxide and nuclear waste, or used for  
49 the extraction of geothermal energy, natural gas, or methane from hydrate accumulations.  
50 Soil moisture balances and the interaction between the subsurface, surface waters, and the  
51 atmosphere are studied on the hillslope, watershed, and global scales. On the other end of  
52 the spectrum, effects such as preferential flow, biogeochemical reactions, and certain  
53 geomechanical behavior occur on much smaller scales that are below the size of a  
54 commonly used computational element or even smaller than the representative  
55 elementary volume as defined in groundwater hydrology.

56 In addition to considering unsaturated flow of water and transport of tracers or non-  
57 reactive components, vadose zone hydrology has evolved to study complex processes of  
58 nonisothermal, multiphase, multicomponent fluid flow coupled to biogeochemical  
59 reactions. The multiscale, multiphysics nature of vadose zone processes poses significant  
60 conceptual and numerical challenges. In addition, advanced measurement techniques and  
61 analysis methods are needed to obtain the characterization data for site-specific models.  
62 Finally, the vadose zone has to be integrated into a larger system, which may include not  
63 only other natural subsystems, but also engineering components as well as economic and  
64 regulatory aspects.

65 The modeling challenges mentioned above can be grouped into three categories:  
66 (1) challenges resulting from the heterogeneity and complexity of the physical and

67 biogeochemical processes occurring in the vadose zone; (2) challenges resulting from the  
68 position of the vadose zone at the interface between different spheres (atmosphere,  
69 biosphere, hydrosphere); and (3) computational challenges resulting from the coupling of  
70 subsystems and processes involving many spatial and temporal scales.

71 The first group of challenges includes the characterization and incorporation of  
72 heterogeneity, which affects flow behavior (fingering, flow focusing, lateral diversion,  
73 preferential and fast flow, water perching) and transport behavior (channelization, plume  
74 spreading). Moreover, biogeochemical reactions not only depend on heterogeneity in  
75 chemical and mineralogical composition, but they are also affected by details of the flow  
76 patterns and transport processes to which they are strongly coupled. Also note that under  
77 unsaturated or multiphase flow conditions, the impact of heterogeneity on these processes  
78 may be self-enhancing or self-controlling, which affects the conceptualization of such  
79 processes in a numerical model.

80 The characterization of heterogeneity is further complicated because the soil structure  
81 may exhibit both systematic and random features on multiple scales. Additionally,  
82 sensors used for monitoring the vadose zone and for measuring its properties have  
83 different support scales, and averaging these properties often leads to effective  
84 parameters that are process-specific, scale-dependent, and anisotropic.

85 The TOUGH simulators have been used extensively to analyze the impact of  
86 heterogeneity on vadose zone processes (Pruess, 1998, 1999, 2004b; Pruess et al., 2002).  
87 Such studies include the use of high-resolution simulations with a massively parallelized  
88 version of the code (Wu et al., 2002; Zhang et al., 2003) and the development of a joint  
89 hydrological-geophysical inversion approach to characterize heterogeneity and to reduce

90 systematic modeling errors (Kowalsky et al., 2005; Finsterle and Kowalsky, 2007;  
91 Lehtikoinen et al., 2007).

92 The classic approach for describing unsaturated flow based on the Richards equation  
93 has been successful but limited. One limitation stems from the difficulty in obtaining  
94 characterization data for specifying the relative permeability and capillary pressure  
95 curves. In addition, the functional form of these curves is difficult to assess and may  
96 greatly impact modeling results. For example, if a standard hysteretic capillary pressure  
97 model is used, key phenomena (such as hysteresis in the relative permeabilities and  
98 history-dependent gas entrapment) may be neglected. The hysteresis model implemented  
99 in TOUGH is presented in Doughty (2007) and will be summarized below. Similarly,  
100 fast-flow through macropores or fractures may be described by an effective continuum  
101 model with multimodal characteristic curves. However, as demonstrated by Doughty  
102 (1999), the applicability of an effective continuum model is limited to cases where the  
103 assumption of thermodynamic equilibrium between the continua is valid. In addition to  
104 the active fracture model by Liu et al. (1998), the TOUGH simulators include dual- and  
105 triple-continuum (Wu et al., 2004) formulations with multiple interacting continua to  
106 accurately capture exchanges of fluids and heat between regions of the porous medium of  
107 vastly different flow and transport characteristics.

108 The vadose zone, being bounded by the land surface and the groundwater table, is in  
109 direct contact with the biosphere and strongly affected by human activities. Interaction  
110 among these various interfaces leads to a second group of modeling challenges. The  
111 processes at the vadose zone boundaries are often highly dynamic (infiltration events,  
112 evapotranspiration, heat transfer, water table fluctuations); more importantly, they may

113 need to be fully coupled to account for feedback mechanisms (e.g., evaporation, root  
114 water uptake). The TOUGH codes accurately account for phase transitions (evaporation  
115 and condensation, including the related latent heat effects) as well as multiphase diffusion  
116 (e.g., of water vapor), allowing the simulation of evaporation and dry-out processes.  
117 Simplified approaches to simulate evaporation using the Richards equation have been  
118 recently implemented (Ghezzehei et al., 2004). TOUGH has also been coupled to the  
119 National Center for Atmospheric Research (NCAR) Community Land Model CLM3  
120 (<http://www.cgd.ucar.edu/tss/clm/index.html>) for the simulation of energy and moisture  
121 dynamics between the atmosphere and the subsurface (Pan et al., 2007). Finally,  
122 integration of TOUGH2 and iTOUGH2 into the GoldSim model (GoldSim Technology  
123 Group, 2006) provides the means to study the interaction between the subsurface  
124 environment and related natural and engineered components on a system level (Zhang et  
125 al., 2007).

126 The third group of challenges is related to the computational difficulties in dealing  
127 with highly nonlinear, coupled processes that occur on multiple scales and with  
128 potentially different characteristic time constants. Spatial discretization in the TOUGH  
129 codes is based on the integral finite difference approach (Narasimhan and Witherspoon,  
130 1976), in which the basic mass conservation equations are directly discretized in their  
131 integral form (Pruess et al., 1999; Pruess, 2004a). This scheme provides great flexibility  
132 in handling complex geometries, multiregion approaches, and a variety of boundary  
133 conditions. Higher-order schemes have also been implemented (Pruess, 1991b;  
134 Oldenburg and Pruess, 2000). Nonlinearities are treated using Newton-Raphson iterations  
135 with a residual-based convergence criterion. Parallelization of the forward (Wu et al.,

136 2002) and inverse (Finsterle, 1998) runs help make tractable the solution of larger  
137 simulation and optimization problems. Nevertheless, phase changes, strong nonlinearities  
138 in characteristic curves near residual saturations, sharp saturation and reaction fronts, and  
139 the coupling of counteracting processes on disparate scales are among the features  
140 causing numerical difficulties that require careful attention by the code developer and  
141 sometimes case-by-case intervention by the user.

142 The remainder of this review article discusses a few select capabilities recently  
143 implemented in various TOUGH modules. These examples address diverse issues from  
144 all three groups of challenges related to vadose zone modeling mentioned above.

## 145 **SELECT CAPABILITIES AND APPLICATIONS**

### 146 **Hysteresis with Gas Entrapment**

147 Numerical modeling has been used extensively in the past few years to study geologic  
148 storage of CO<sub>2</sub> in brine-saturated formations. At depths commonly considered for CO<sub>2</sub>  
149 storage (>800 m), CO<sub>2</sub> primarily exists as a gas-like supercritical phase, which is the non-  
150 wetting phase, while some CO<sub>2</sub> dissolves in the brine, which is the wetting phase.  
151 Interactions between the two fluid phases are represented at the grid-block scale by  
152 capillary pressure and relative permeability functions. The amount of CO<sub>2</sub> potentially  
153 trapped in the subsurface depends on hysteresis effects. Given the underlying trapping  
154 mechanism, it is necessary to develop a hysteresis model that is capable of simulating  
155 history-dependent gas entrapment.

156 During periods of CO<sub>2</sub> injection into brine-saturated formations, the resulting CO<sub>2</sub>  
157 plume grows continuously, that is, all locations follow the primary drainage branch of the  
158 capillary pressure curve at all times, and this branch can be replicated using a non-  
159 hysteretic formulation. However, for post-injection periods, when the CO<sub>2</sub> plume moves  
160 upward and updip due to buoyancy forces, different locations experience drainage and  
161 imbibition at different times, necessitating the use of a hysteretic formulation.

162 In a hysteretic model, some parameters depend only on the process (drainage or  
163 imbibition) that is occurring, so it is convenient to subdivide the characteristic curves into  
164 drainage branches and imbibition branches (see Figure 2 below). The parameters  
165 describing gas entrapment, however, depend on the value of the saturation when the grid  
166 block makes a transition from drainage to imbibition or vice versa, the so-called turning-  
167 point saturations. Because turning-point saturations are different in each grid block, these  
168 parameters are spatially variable and history-dependent. The most critical parameter is  
169 the residual gas saturation, denoted  $S_{gr}^{\Delta}$ , which is the saturation below which gas is  
170 immobile (i.e., the saturation below which immiscible CO<sub>2</sub> is trapped). For the primary  
171 drainage curve,  $S_{gr}^{\Delta} = 0$ , but for imbibition,  $S_{gr}^{\Delta}$  increases as the liquid saturation at the  
172 drainage-to-imbibition turning point, denoted  $S_l^{\Delta}$ , decreases. Thus, grid blocks that once  
173 contained the most CO<sub>2</sub> are those which trap the most CO<sub>2</sub>. The maximum possible  
174 value of  $S_{gr}^{\Delta}$  is  $S_{grmax}$ , which is obtained for the minimum possible value of  $S_l^{\Delta}$ ; this  
175 minimum turning-point saturation is generally equal to the irreducible liquid saturation  
176  $S_{lr}$ . The value of  $S_{gr}^{\Delta}$  determines the history- and location dependent amount of CO<sub>2</sub> that  
177 can be trapped. Note that gas entrapment cannot be adequately simulated using a model



178 that is solely based on the Richards equation, in which gas is considered a passive  
179 bystander; a two-phase formulation is needed (Faybishenko, 1995).

180 We consider an application in which CO<sub>2</sub> is injected into a porous formation 100 m  
181 thick located at a depth of 1,000 m. This system is represented by an axisymmetric model  
182 with the injection well in the center. The porosity of the formation is 25%, horizontal  
183 permeability is  $2 \times 10^{-13}$  m<sup>2</sup>, and vertical permeability is  $1 \times 10^{-13}$  m<sup>2</sup>. The overburden  
184 above the storage formation extends to the surface and is assumed to have the same  
185 properties as the storage formation itself; thus, there is no low-permeability caprock.  
186 Initially, the brine saturation is 100% everywhere in the model, pore pressure is  
187 hydrostatic with a pressure of 1 bar at the surface, and temperature follows the  
188 geothermal gradient of 30 °C/km, with the temperature at the surface and base of the  
189 model held constant at 15 °C and 45 °C, respectively. The salinity of the pore water is  
190 assumed to be 100,000 ppm. Fluid and heat flow are fully coupled in the simulations.

191 The numerical simulations begin with injection of 900,000 tons of CO<sub>2</sub> into the porous  
192 formation at a constant rate of 30,000 tons per day for one month. (This rate of CO<sub>2</sub>  
193 corresponds roughly to emissions of a 1,000 MW coal-fired power plant.) After injection  
194 stops, the only driving force in the model tending to cause movement of the CO<sub>2</sub> is  
195 buoyancy. Simulations continue for 1,000 years.

196 Figure 1 shows the CO<sub>2</sub> plume at a series of times. During the one-month injection  
197 period, the CO<sub>2</sub> plume is expanding in all directions, and the hysteretic-model results do  
198 not differ from what would be obtained with a non-hysteretic model. Thereafter, the  
199 leading edge of the plume, where drainage occurs and  $S_{gr}$  is zero, continues to advance  
200 (reaching the surface at about 700 years), while the trailing edge of the plume, where

201 imbibition occurs and  $S_{gr}$  is large, remains largely trapped. This combination of processes  
202 cannot be replicated with a non-hysteretic model or a hysteretic model that does not  
203 include phase trapping. If a non-hysteretic model with a small value of  $S_{gr}$  is used, most  
204 of the plume escapes through the ground surface within 10 years; whereas a non-  
205 hysteretic model with a large value of  $S_{gr}$  produces a plume that never reaches the surface  
206 and remains entirely trapped indefinitely.

207 Figure 2 shows the capillary pressure and relative permeability paths followed for  
208 several locations in the CO<sub>2</sub> plume. All paths begin at  $S_l = 1$  along the primary drainage  
209 curve; the transition to an imbibition scanning curve occurs at  $S_l^\Delta$  (shown by arrows); as  
210  $|P_c| \rightarrow 0$  and  $k_{rg} \rightarrow 0$  on the imbibition curves,  $S_l \rightarrow (1 - S_{gr}^\Delta)$  (shown by black-outlined  
211 dots). Thus grid blocks near the plume center, which get much drier during the injection  
212 period and therefore have a small  $S_l^\Delta$ , have a much larger  $S_{gr}^\Delta$ , and consequently trap  
213 more CO<sub>2</sub> than do grid blocks barely reached by the plume. More details about this  
214 modeling capability and the related application can be found in Doughty (2007).

## 215 **Hydrological Processes in Permafrost**

216 Subsurface flow is governed by the characteristics of the porous medium, the fluid  
217 properties, and constitutive relations describing the interaction between the porous  
218 medium and the fluids. The equation-of-state modules of the TOUGH codes provide an  
219 accurate description of the thermophysical properties of the considered fluid mixtures.  
220 Specifically, the properties of water are calculated within experimental accuracy from  
221 steam table equations as given by the International Formulation Committee (IFC, 1967).

222 As part of the ongoing re-engineering of TOUGH, the temperature and pressure range  
223 available for the calculation of water properties has been expanded to include the phase  
224 transition from liquid or gas to ice and vice versa. The enthalpy, sublimation pressure, as  
225 well as fusion and melting pressures of ice (on the ice-vapor and ice-liquid equilibrium  
226 lines of the water phase diagram) are computed using regression equations from data  
227 obtained by the National Institute for Science and Technology. Within the ice phase (to  
228  $T = 50$  K and  $P \approx 200$  MPa), ice densities are determined using the ice compressibility  
229 model of Marion and Jakubowski (2004) and the thermal expansivity data from Tanaka  
230 (1999). The ice enthalpy is computed using the heat capacity polynomial equation with  
231 the coefficients reported in Yaws (1999). Changes in fluid capillary pressure and relative  
232 permeability relations as a function of ice saturation are also accounted for.

233 Simulating freezing and melting processes is essential to improve our understanding of  
234 permafrost regions (e.g., to study the hydrological response to climate change). These  
235 processes also occur during the formation and dissociation of gas hydrates deposited in  
236 permafrost and sub-oceanic formations (Moridis, 2003; Moridis et al., 2005). The  
237 extended equation-of-state for water is implemented in the re-engineered version of  
238 TOUGH2, named TOUGH+. To demonstrate the capability of the TOUGH+GasH2O  
239 code to handle melting ice and steam fronts in a single model, we simulated the extreme  
240 thermal conditions encountered when a heat-generating power-source (e.g., from a  
241 landing vehicle) is buried into permafrost on Mars. A heat source of 250 W is assumed to  
242 be embedded in the shallow Martian subsurface. Below a depth of 0.2 m, the pore space  
243 contains 50% ice and 50% carbon dioxide at an atmospheric pressure of only 713 Pa and  
244 a temperature of  $-80$  °C; above the permafrost is a layer of completely dry sediment.

245 Figure 3 shows the distribution of temperature, water and ice saturations after 10 sols  
246 (“Martian days;” 1 sol = 88,620 sec). In the immediate vicinity of the heat source the ice  
247 has been melted and the water vaporized. Liquid water only exists in a relatively thin  
248 region with temperatures between about 0 and 60 °C. At the outer edge of this region, the  
249 water freezes, creating an ice barrier that effectively prevents convective heat transport in  
250 radial direction. Water vapor (and associated thermal energy) is redirected upwards  
251 where it escapes to the Martian atmosphere. The simulations predict that the zone  
252 disturbed by a buried heat source is very limited. Specifically, liquid water is confined to  
253 a narrow region, reducing the risk that terrestrial microorganisms that may have been  
254 carried by the landing vehicle could survive and proliferate. More details about this  
255 simulation study can be found in Moridis and Pruess (2006).

## 256 **Biogeochemical Reactions**

257 Understanding and predicting the fate of nutrients and contaminants in the vadose  
258 zone requires simulation of biogeochemical reactions. Accounting for biogeochemical  
259 reactions is also important because most redox reactions occurring in the shallow  
260 subsurface are catalyzed by bacteria. Geochemical and microbiological reactions are  
261 strongly coupled to flow and transport processes, and—depending on the scale at which  
262 they are studied—may not reach local equilibrium and thus require kinetic rate laws. A  
263 multi-regional formulation for intra-aqueous kinetic reactions and biodegradation has  
264 been incorporated into TOUGHREACT (Xu and Pruess, 2001; Xu et al., 2006), which  
265 considers a variety of subsurface thermo-physical-chemical processes for a wide range of  
266 hydrological and chemical conditions. Interactions between mineral assemblages and

267 fluids can be modeled assuming local equilibrium or kinetics. The gas phase may be  
268 chemically active, and precipitation and dissolution reactions may change formation  
269 porosity and permeability. Reactions among primary species (including intra-aqueous and  
270 sorption reaction kinetics and biodegradation) are described using a general rate law that  
271 accounts for multiple mechanisms and multiple products, concentration-dependent  
272 (Monod) rate expressions, and inhibition terms.

273         Since most bacteria grow within a relatively immobile biofilm on solid surfaces, a  
274 three-region model is proposed that consists of (1) a mobile region, (2) an immobile  
275 region, which includes stagnant water and biomass, and (3) a solid particle region where  
276 mineral dissolution or precipitation and surface reactions may occur (Figure 4). Instead of  
277 explicitly considering every pore and particle, the three regions are lumped into three  
278 overlapping continua, which are discretized separately and connected to each other. If  
279 necessary, each region can be further discretized to better resolve steep gradients and  
280 sharp reaction fronts. This concept is similar to the MINC model (multiple interacting  
281 continua; Pruess and Narasimhan (1985)) and the triple-continuum approach of Wu et al.  
282 (2004), both implemented in the TOUGH simulators. These models resolve global fluid  
283 and heat flow through a fractured (or macropore) system, while accounting for the local  
284 exchange between the fractures and the matrix. The extension of the MINC method to  
285 reactive geochemical transport is described in Xu and Pruess (2001).

286         Reactive transport of denitrification was simulated using both a single-continuum and  
287 a multi-region model, and the results are compared to data from the column experiments  
288 of von Gunten and Zobrist (1993). While the single-continuum model fails to reproduce  
289 the nitrate concentration profiles, the multi-region model (see Figure 5) captures the

290 system behavior reasonably well, even though the volume of the immobile region needed  
291 to be increased (potentially reflecting bacterial growth) at later times.

292 The biogeochemical transport simulation capabilities of TOUGHREACT will be  
293 useful for many subsurface problems, including acid mine drainage remediation, organic  
294 matter decomposition, oil and gas maturation, sulfite reduction in oil fields, and effective  
295 environmental remediation of groundwater contamination. More details about  
296 TOUGHREACT and its applications can be found in Xu and Pruess (2001), Xu et al.  
297 (2001), and Xu (2007).

## 298 **Parameter Estimation and Model Structure Identification**

299 An accurate description of physical processes, biogeochemical reactions, and fluid  
300 properties is a prerequisite for a reliable prediction of vadose zone systems. However, a  
301 major source of prediction uncertainty lies in our incomplete knowledge of the subsurface  
302 structure and the related soil properties. The complexity of soil formation as well as  
303 depositional and erosional processes result in an equally complex, usually highly  
304 heterogeneous, but not entirely random subsurface structure. While several stochastic  
305 methods exist to describe and simulate subsurface structures (using, for example,  
306 geostatistics (Deutsch and Journel, 1992) or lithofacies modeling (Carle and Fogg,  
307 1996)), the determination of the actual structure at a given site remains challenging. In  
308 addition to identifying the geometry of the stratal soil architecture, hydrogeologic and  
309 geochemical parameters need to be assigned. These parameters are often scale-dependent,  
310 specific to the process being simulated, and related to other aspects of the conceptual  
311 model. Finally, initial and boundary conditions are either unknown or uncertain, so they

312 need to be parameterized and estimated along with the structure and soil properties.  
313 Inverse modeling is a means to obtain parameters that in some sense can be considered  
314 optimal for a given model. However, it is important to realize that an error in the  
315 conceptual model can yield parameter estimates that are biased or even meaningless; it is  
316 therefore essential to address the impact of systematic errors (in the data and the  
317 conceptual model) when calibrating a vadose zone model.

318 The iTOUGH2 code (Finsterle, 2004; <http://www-esd.lbl.gov/iTOUGH2>) provides  
319 inverse modeling capabilities for most modules of the TOUGH suite of simulators.  
320 iTOUGH2 solves a nonlinear optimization problem to determine TOUGH input  
321 parameters based on measured data for which corresponding TOUGH output is  
322 calculated. This means that any aspect of the model that can be parameterized—including  
323 boundary conditions and the soil structure—can be subjected to estimation by inverse  
324 modeling. Moreover, standard TOUGH output variables can be used to calculate new  
325 quantities that can then define the objective for optimization—including geophysical data  
326 or also costs.

327 This flexibility has been exploited to develop a joint inversion approach, in which  
328 hydrological and geophysical data are inverted to estimate hydrogeological,  
329 geostatistical, and petrophysical parameters (Kowalsky et al., 2004; 2005; Finsterle and  
330 Kowalsky, 2007). In this approach, the potential estimation bias introduced by a  
331 systematic error in the conceptual model (specifically in the representation of subsurface  
332 heterogeneity) is reduced by adjusting the model structure itself during the optimization  
333 process. The increased need for data that contain information about the subsurface  
334 structure is met by adding geophysical data. The inclusion of hydrogeological data in the

335 joint inversion approach ensures that a relation can be established between the  
336 geophysical signals and soil properties that determine fluid flow (note that this may  
337 require the estimation of additional parameters, such as those of a petrophysical  
338 relationship). An example is shown in Figure 6, where a highly heterogeneous,  
339 anisotropic soil structure and its related properties are determined by the joint inversion  
340 of hydrological data (infiltration rates and neutron probe measurements) and geophysical  
341 data (arrival times from a cross-hole ground penetrating radar survey). Details about this  
342 specific application can be found in Finsterle and Kowalsky (2007).

343 Since inverse modeling usually deals with the difference between the measured and  
344 calculated system response, systematic errors may stem from errors in both the data and  
345 the model, and it is often difficult (and sometimes irrelevant) to distinguish between the  
346 two sources. For example, data from laboratory experiments may show a systematic  
347 deviation (trend) from the expected behavior. If the trend is a result of a leak in the  
348 testing apparatus, it can be considered a data error, or an error in the model, as the model  
349 does not properly represent the experimental conditions. Depending on the statistical  
350 properties of the residuals, the problem can be resolved using robust estimators (Finsterle  
351 and Najita, 1997), through explicit simulation of the processes expected to have  
352 influenced the data and associated parameter estimation (Finsterle and Persoff, 1997),  
353 through the estimation of a correction parameter (Kowalsky et al., 2005), or through the  
354 development of a statistical approximation error model (Lehikoinen et al., 2007). All  
355 these approaches are being examined in the context of vadose zone characterization using  
356 the TOUGH suite of forward and inverse models.



## 357 **Coupling with Other Models**

358 Since the vadose zone is in direct contact with the land surface, it is essential to  
359 consider hydrologic and chemical interactions between the atmosphere, land surface, and  
360 subsurface. In addition, anthropogenic activities (such as land cultivation, irrigation,  
361 hydraulic engineering projects, waste disposal) may profoundly affect the vadose zone  
362 and other related natural systems. These coupled impacts on the water and chemical  
363 cycles also influence (and are influenced by) the economic and regulatory environment.

364 Considering the vadose zone as a disconnected subsystem raises difficult questions  
365 regarding the boundary conditions to be employed at the land surface. While net  
366 infiltration can be estimated using experimentally based parameterization models (for a  
367 review, see Faybishenko (2007)), evapotranspiration (a potentially significant contributor  
368 to the moisture balance at the surface, specifically in arid regions) is a coupled process  
369 that requires a physical description of both surface and subsurface conditions.  
370 Conversely, land hydrologic responses to meteorological forcing involve complicated  
371 exchanges of moisture and energy between soil, vegetation, snowpack, groundwater, and  
372 the overlying atmospheric boundary layer. The NCAR Community Land Model CLM3 is  
373 a model primarily developed to meet the needs of regional climate modeling. In CLM3,  
374 radiation, sensible and latent heat transfer, zonal and meridional surface stresses, and  
375 ecological and hydrological processes are simulated as interrelated subprocesses.  
376 However, the subsurface moisture flow in CLM3 is only considered in a simplified  
377 manner. CLM3 has been coupled to TOUGH2 through an internal interface that includes  
378 flux and state variables shared by the two submodels. Specifically, TOUGH2 uses  
379 infiltration, evaporation, and root-uptake rates, calculated by CLM3, as sink or source

380 terms, while CLM3 uses saturation and capillary pressure profiles, calculated by  
381 TOUGH2, as state variables.

382 Simulation results show (see Figure 7) that the coupled model greatly improves the  
383 prediction of water table elevation, evapotranspiration, surface temperature, and soil  
384 moisture, as evaluated using 18 years of data observed at a real site (Pan et al., 2007).  
385 The new model can be extended to include an atmospheric simulation model to simulate  
386 hydraulic processes from the top of the atmosphere to deep in the ground.

387 In addition to coupling atmospheric, land surface, and subsurface processes, the  
388 vadose zone is linked to many other environmental and engineered systems. The  
389 interaction among these subsystems can be better understood, analyzed, and optimized  
390 using a system-level modeling tool such as GoldSim (GoldSim Technology Group, 2006;  
391 <http://www.goldsim.com>). For example, decisions regarding the use of biofuels as an  
392 alternative energy source need to be based on an analysis of the interactions between  
393 regional hydrological cycles, water and energy needs for biofuel production, impacts on  
394 the vadose zone and groundwater resources, as well as economic and regulatory  
395 parameters. Uncertainties and risks associated with each submodel and its parameters  
396 also need to be evaluated. To support system-level studies involving subsurface flow and  
397 transport processes, both TOUGH2 and iTOUGH2 have been linked to GoldSim. This  
398 coupling provides the capability to simulate the interaction between the vadose zone and  
399 various engineered components, to analyze the economic impact of environmental  
400 management decisions, to perform risk analysis studies, and to optimize testing and  
401 monitoring designs. Moreover, GoldSim provides a convenient graphical interface to  
402 control TOUGH simulations and to visualize modeling results. Figure 8 shows an

403 example of a TOUGH-GoldSim application that focuses on evaluating the feasibility of  
404 carbon sequestration with enhanced gas recovery, where the economic benefits of  
405 enhanced methane production is directly weighed against the costs and benefits of CO<sub>2</sub>  
406 capture and injection. In this example, the reservoir simulations are performed using a  
407 module for multicomponent gas mixtures of methane and CO<sub>2</sub> (Oldenburg et al., 2004).  
408 More details about this application can be found in Zhang et al. (2007).

409 Finally, the integration of a subsurface process simulator into a system-level modeling  
410 tool that also includes an economic model provides an opportunity to evaluate and  
411 optimize water management decisions. Optimization routines provided by GoldSim or  
412 iTOUGH2 can also be used to determine operational parameters of a remediation project  
413 (an example is discussed in Finsterle (2005)).

#### 414 **CONCLUDING REMARKS**

415 To understand and predict the response of the vadose zone to naturally occurring  
416 hydrological events or anthropogenic interference requires the use of sophisticated  
417 numerical modeling capabilities. The TOUGH suite of simulators is well suited to  
418 address the conceptual and computational challenges that are specific to unsaturated  
419 subsurface systems. The accurate process description implemented in TOUGH provides  
420 the basis for the analysis of the vadose zone and its interactions with other subsystems.  
421 However, we believe that an integrated approach to site characterization and predictive  
422 modeling is needed to reduce the impact of systematic modeling errors on our forecast of  
423 vadose zone system behavior.

424 **ACKNOWLEDGMENT**

425 We would like to thank Jonny Rutqvist (LBNL) for his careful review of the  
426 manuscript. This work was supported by the U.S. Dept. of Energy under Contract No.  
427 DE-AC02-05CH11231.

428 **REFERENCES**

- 429 Carle, S. F., and G. E. Fogg. 1996. Transition probability-based geostatistics. *Math. Geol.*  
430 28(4):453-476.
- 431 Deutsch, C. V., and A. G. Journel. 1992. *GSLIB-Geostatistical Software Library and*  
432 *User's Guide*. Oxford University Press, New York.
- 433 Doughty, C. 1999. Investigation of conceptual and numerical approaches for evaluating  
434 moisture, gas, chemical, and heat transport in fractured unsaturated rock. *Journal of*  
435 *Contaminant Hydrology* 38:69–106.
- 436 Doughty, C. 2007. Modeling geologic storage of carbon dioxide: comparison of non-  
437 hysteretic and hysteretic characteristic curves. *Energy Conversion and Management*  
438 (in press).
- 439 Falta, R. W., K. Pruess, S. Finsterle, and A. Battistelli. 1995. *T2VOC User's Guide*. Rep.  
440 LBL-36400, Lawrence Berkeley Lab., Berkeley, California.
- 441 Faybishenko, B. A., 1995. Hydraulic behavior of quasi-saturated soils in the presence of  
442 entrapped air: Laboratory experiments. *Water Resour. Res.*, 31(10), 2421–2436,  
443 10.1029/95WR01654.
- 444 Faybishenko, B. 2007. Climatic forecasting of net infiltration at Yucca Mountain using  
445 analogue meteorological data. *Vadose Zone J.* 6:77–92.

446 Finsterle, S. 1998. Parallelization of iTOUGH2 using PVM. Rep. LBNL-42261,  
447 Lawrence Berkeley Natl. Lab., Berkeley, California.

448 Finsterle, S. 1999a. iTOUGH2 user's guide. Rep. LBNL-40040, Lawrence Berkeley Natl.  
449 Lab., Berkeley, California.

450 Finsterle, S. 1999b. iTOUGH2 command reference. Rep. LBNL-40041, Lawrence  
451 Berkeley Natl. Lab., Berkeley, California.

452 Finsterle, S. 1999c. iTOUGH2 sample problems. Rep. LBNL-40042, Lawrence Berkeley  
453 Natl. Lab., Berkeley, California.

454 Finsterle, S. 2004. Multiphase inverse modeling: Review and iTOUGH2 applications.  
455 *Vadose Zone J.* 3:747–762.

456 Finsterle, S. 2005. Demonstration of optimization techniques for groundwater plume  
457 remediation using iTOUGH2. *Environmental Modelling and Software* (21)5:665–  
458 680, doi:10.1016/j.envsoft.2004.11.012.

459 Finsterle, S., and P. Persoff. 1997. Determining permeability of tight rock samples using  
460 inverse modeling. *Water Resour. Res.*, 33(8): 1803–1811.

461 Finsterle, S., and J. Najita. 1998. Robust estimation of hydrogeologic model parameters.  
462 *Water Resour. Res.* 34(11):2939–2947.

463 Finsterle, S., and M. B. Kowalsky. 2007. Joint hydrological-geophysical inversion for  
464 soil structure identification. *Vadose Zone J.* (in press).

465 Ghezzehei, T. A., R. C. Trautz, S. Finsterle, P. J. Cook, and C. F. Ahlers. 2004. Modeling  
466 coupled evaporation and seepage in ventilated tunnels, *Vadose Zone J.*, 3:806–818.

467 GoldSim Technology Group. 2006. GoldSim User's Guide. <http://www.goldsim.com>.

468 International Formulation Committee. 1967. A formulation of the thermodynamic  
469 properties of ordinary water substance. IFC Secretariat, Düsseldorf, Germany.

470 Kowalsky, M.B., S. Finsterle, and Y. Rubin. 2004. Estimating flow parameter  
471 distributions using ground-penetrating radar and hydrological measurements during  
472 transient flow in the vadose zone. *Adv. Water Resour.* 27(6):583–599.

473 Kowalsky, M., S. Finsterle, J. Peterson, S. Hubbard, Y. Rubin, E. Majer, A. Ward, and G.  
474 Gee. 2005. Estimation of field-scale soil hydraulic parameters and dielectric  
475 parameters through joint inversion of GPR and hydrological data. *Water Resour. Res.*  
476 41, W11425, doi:10.1029/2005WR004237.

477 Lehtikainen, A., S. Finsterle, A. Voutilainen, L. M. Heikkinen, M. Vauhkonen, and J. P.  
478 Kaipio. 2007. Approximation errors and truncation of computational domains with  
479 application to geophysical tomography, *Inverse Problems and Imaging*, 1(2):371–  
480 389.

481 Liu, H.H., C. Doughty, and G. S. Bodvarsson. 1998. An active fracture model for  
482 unsaturated flow and transport in fractured rocks. *Water Resour. Res.* 34(10):2633–  
483 2646.

484 Marion, G.M., and Jakubowski, S.D. 2004. The compressibility of ice to 2.0 kbar. *Cold  
485 Regions Science and Technology* 38(2–3):211–218.

486 Moridis, G.J. 2003. Numerical studies of gas production from methane hydrates. *SPE  
487 Journal* 32(8):359–370.

488 Moridis, G.J., M.B. Kowalsky, and K. Pruess. 2005. Depressurization-induced gas  
489 production from class 1 hydrate deposits. SPE 97266, presented at 2005 Annual  
490 Technical Conference and Exhibition, Dallas, Texas, October 9–12, 2005.

491 Moridis, G.J, and K. Pruess. 2006. TOUGH+/GasH2O study of the effects of a heat  
492 source buried in the Martian permafrost. Proceedings, TOUGH Symposium 2006,  
493 Rep. LBNL-60087, Lawrence Berkeley Natl. Lab., Berkeley, California.

494 Narasimhan, T.N., and P.A. Witherspoon. 1976. An integrated finite difference method  
495 for analyzing fluid flow in porous media. *Water Resour. Res.* 12:57–64.

496 Oldenburg, C.M., and K. Pruess. 2000. Simulation of propagating fronts in geothermal  
497 reservoirs with the Implicit Leonard Total Variation Diminishing Scheme.  
498 *Geothermics* 29:1–25.

499 Oldenburg, C.M., G.J. Moridis, N. Spycher, and K. Pruess K. 2004. EOS7C, version 1.0:  
500 TOUGH2 module for carbon dioxide or nitrogen in natural gas (methane) reservoirs.  
501 Rep. LBNL-56589, Lawrence Berkeley Natl. Lab., Berkeley, California.

502 Pan, L., J. Jin, N. Miller, Y.-S. Wu, and G.S. Bodvarsson. 2007. Modeling hydraulic  
503 responses to meteorological forcings: from canopy to aquifer. *Vadose Zone J.*  
504 (accepted).

505 Pruess, K. 1991a. TOUGH2—A general-purpose numerical simulator for multiphase  
506 fluid and heat flow. Rep. LBL-29400, Lawrence Berkeley Lab., Berkeley, California.

507 Pruess, K. 1991b. Grid orientation and capillary pressure effects in the simulation of  
508 water injection into depleted vapor zones. *Geothermics* 20(5/6):257–277.

509 Pruess, K. 1998. On Water Seepage and Fast Preferential Flow in Heterogeneous,  
510 Unsaturated Rock Fractures. *J. Contam. Hydr.*, 30(3–4):333–362.

511 Pruess, K. 1999. A mechanistic model for water seepage through thick unsaturated zones  
512 in fractured rocks of low matrix permeability. *Water Resour. Res.*, 35(4):1039–1051.

513 Pruess, K. 2004a. The TOUGH codes—a family of simulation tools for multiphase flow  
514 and transport processes in permeable media. *Vadose Zone J.* 3:738–746.

515 Pruess, K. 2004b. A composite medium approximation for unsaturated flow in layered  
516 sediments. *J. Contam. Hydr.* 70(3–4):225–247, doi:10.1016/j.jconhyd.2003.09.007.

517 Pruess, K., and Narasimhan, T. N. 1985. A practical method for modeling fluid and heat  
518 flow in fractured porous media. *Society of Petroleum Engineers Journal* 25:14–26.

519 Pruess, K., C. Oldenburg, and G. Moridis. 1999. TOUGH2 user’s guide, Version 2.0.  
520 Rep. LBNL-43134, Lawrence Berkeley Natl. Lab., Berkeley, California.

521 Pruess, K., and A. Battistelli. 2002. TMVOC, a numerical simulator for three-phase non-  
522 isothermal flows of multicomponent hydrocarbon mixtures in saturated-unsaturated  
523 heterogeneous media. Rep. LBNL-49375, Lawrence Berkeley Natl. Lab., Berkeley,  
524 California.

525 Pruess, K., S. Yabusaki, C. Steefel and P. Lichtner. 2002. Fluid Flow, Heat Transfer, and  
526 Solute Transport at Nuclear Waste Storage Tanks in the Hanford Vadose Zone.  
527 *Vadose Zone J.* 1(1–2):68–88.

528 Richards, L. H. 1931. Capillary conduction of liquids through porous mediums. *Physics*  
529 1:318–333.

530 Rutqvist J., Y.-S. Wu, C.-F. Tsang, and G. Bodvarsson. 2002. A modeling approach for  
531 analysis of coupled multiphase fluid flow, heat transfer, and deformation in fractured  
532 porous rock *Int. J. Rock Mech. & Min. Sci.* 39:429–442.

533 Tanaka, H. 1999. Thermal expansivities of cubic ice I and ice VII. *Journal of Molecular*  
534 *Structure (Theochem)* 461–462:561–567.



535 von Gunten, U., and Zobrist, J. 1993. Biogeochemical changes in groundwater infiltration  
536 systems: column studies. *Geochim. Cosmochim. Acta* 57:3895–3906.

537 Wu, Y.S., K. Zhang, C. Ding, K. Pruess, E. Elmroth, and G.S. Bodvarsson. 2002. An  
538 efficient parallel-computing method for modeling nonisothermal multiphase flow and  
539 multicomponent transport in porous and fractured media. *Adv. Wat. Resour.* 25:243–  
540 261.

541 Wu, Y. S., H. H. Liu, and G. S. Bodvarsson. 2004. A triple-continuum approach for  
542 modeling flow and transport processes in fractured rock. *Journal of Contaminant*  
543 *Hydrology* 73:145–179.

544 Xu, T., and K. Pruess. 2001. Modeling multiphase non-isothermal fluid flow and reactive  
545 geochemical transport in variably saturated fractured rocks: 1. Methodology,  
546 *American Journal of Science* 301:16–33.

547 Xu, T., E. Sonnenthal, N. Spycher, K. Pruess, G. Brimhall, and J. Apps. 2001. Modeling  
548 multiphase non-isothermal fluid flow and reactive geochemical transport in variably  
549 saturated fractured rocks: 2. Applications to supergene copper enrichment and  
550 hydrothermal flows, *American Journal of Science* 301:34–59.

551 Xu, T., E.L. Sonnenthal, N. Spycher, and K. Pruess. 2004. TOUGHREACT user's guide:  
552 A simulation program for non-isothermal multiphase reactive geochemical transport  
553 in variably saturated geologic media. Rep. LBNL-55460, Lawrence Berkeley Natl.  
554 Lab., Berkeley, California.

555 Xu, T., E.L. Sonnenthal, N. Spycher, and K. Pruess. 2006. TOUGHREACT: A  
556 simulation program for non-isothermal multiphase reactive geochemical transport in  
557 variably saturated geologic media. *Computer & Geoscience* 32(2):145–165.

558 Xu, T. 2007. Incorporation of aqueous reaction kinetics and biodegradation into  
559 TOUGHREACT: Application of a multi-region model to hydrobiogeochemical  
560 transport of denitrification and sulfate reduction. *Vadose Zone J.* (in press).

561 Yaws, C.L. 1999. *Chemical properties handbook: physical, thermodynamic,*  
562 *environmental, transport, safety, and health related properties for organic and*  
563 *inorganic chemicals.* McGraw-Hill. New York, New York.

564 Zhang, K., Y. S. Wu, and G. S. Bodvarsson. 2003. Massively parallel computing  
565 simulation of fluid flow in the unsaturated zone of Yucca Mountain, Nevada. *Journal*  
566 *of Contaminant Hydrology* 62–63:381–399.

567 Zhang, Y. C. M. Oldenburg, S. Finsterle, and G. S. Bodvarsson. 2007. System-level  
568 modeling for economic evaluation of geological CO<sub>2</sub> storage in gas reservoirs.  
569 *Energy Conservation and Management*, doi:10.1016/j.enconman.2007.01.018.

570

570 **Table 1. The TOUGH suite of simulators: Main codes**

<b>Simulator</b>	<b>Comment</b>	<b>Reference</b>
<b>TOUGH2</b>	<b>General-purpose simulator for nonisothermal two-phase systems</b>	<b>Pruess, 1991a</b>
<b>T2VOC</b>	<b>Nonisothermal three-phase simulator for environmental applications</b>	<b>Falta et al., 1995</b>
<b>iTOUGH2</b>	<b>Inverse modeling, sensitivity analysis, and uncertainty propagation analysis for TOUGH2 and T2VOC</b>	<b>Finsterle, 1999a, b, c</b>
<b>TOUGH2 V2.0</b>	<b>Updated version of TOUGH2, with added process descriptions and fluid properties modules</b>	<b>Pruess et al., 1999</b>
<b>TMVOC</b>	<b>Nonisothermal three-phase simulator for multicomponent hydrocarbon mixtures</b>	<b>Pruess and Battistelli, 2002</b>
<b>TOUGH-FLAC</b>	<b>Simulator for coupled nonisothermal multiphase flow and rockmechanical processes</b>	<b>Rutqvist et al., 2002</b>
<b>TOUGHREACT</b>	<b>Simulator for nonisothermal multiphase flow and reactive biogeochemical transport</b>	<b>Xu et al., 2004</b>
<b>TOUGH+</b>	<b>Re-engineered version of TOUGH2 V2.0 with enhanced process descriptions and added fluid property modules</b>	<b>(research code)</b>

571 **Table 2. TOUGH simulation capabilities and applications**

<b>Simulation capability</b>	<b>Application</b>	<b>Reference</b>
<b>Hysteresis with gas entrapment</b>	<b>CO<sub>2</sub> sequestration</b>	<b>Doughty (2007)</b>
<b>Freezing and melting</b>	<b>Ice on Mars</b>	<b>Moridis et al. (2006)</b>
<b>Reactive biogeochemical transport</b>	<b>Denitrification</b>	<b>Xu (2007)</b>
<b>Joint hydrological-geophysical inversion</b>	<b>Vadose zone characterization</b>	<b>Finsterle and Kowalsky (2007); Kowalsky et al. (2004, 2005)</b>
<b>Coupling to land surface model</b>	<b>Watershed moisture prediction</b>	<b>Pan et al. (2007)</b>
<b>Integration into system-level model</b>	<b>Enhanced gas production and CO<sub>2</sub> sequestration</b>	<b>Zhang et al. (2007)</b>

572

573

573 **FIGURE CAPTIONS**

574 Figure 1. CO<sub>2</sub> plume evolution (from Doughty, 2007). The single black contour line  
575 shows  $S_g = 0$ . The colored points identify the locations for which characteristic  
576 curves are shown in Figure 2.

577 Figure 2. Hysteretic capillary pressure (top) and relative permeability (bottom) paths for  
578 several grid blocks within the CO<sub>2</sub> plume (from Doughty, 2007). Grid-block  
579 locations are shown in Figure 1. All paths start at  $S_l = 1$  on the primary drainage  
580 curve.

581 Figure 3. Simulation of heat source buried in Martian permafrost (from Moridis and  
582 Pruess, 2006). (a) temperature, (b) water saturation, and (c) ice saturation after 10  
583 sols.

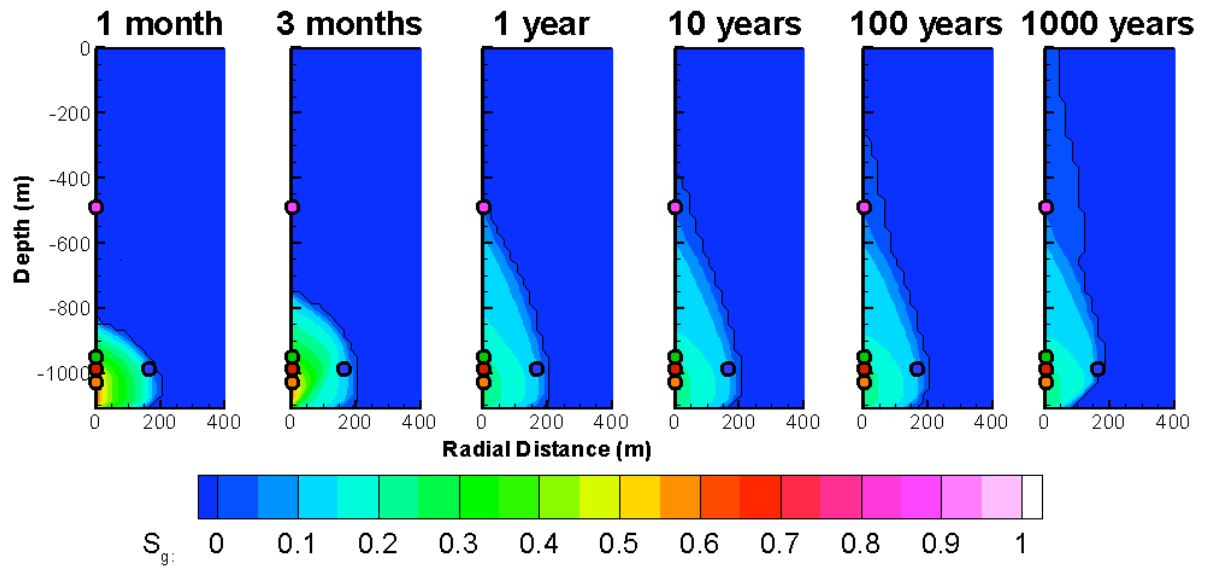
584 Figure 4. Schematic representation of a multi-region model for resolving local diffusive  
585 transport (from Xu, 2007).

586 Figure 5. Nitrate concentrations obtained with the multi-region model after 7 and 14 days  
587 (from Xu, 2007); measured data are from von Gunten and Zobrist (1993).

588 Figure 6. Demonstration of joint hydrological-geophysical inversion approach for soil  
589 structure identification (from Finsterle and Kowalsky, 2007). (a) Liquid saturation  
590 distribution after one day of water release, locations of neutron probes in boreholes  
591 (squares), and GPR straight-ray paths used for inversion; (b) site-specific  
592 permeability field obtained by the joint estimation of geostatistical, hydrogeological,  
593 and petrophysical parameters.

594 Figure 7. Comparison between observed and simulated daily water tables using CLM3  
595 and the coupled CLM3-TOUGH2 simulators (from Pan et al., 2007).

596 Figure 8. System-level model for the evaluation of carbon sequestration with enhanced  
597 gas recovery (from Zhang et al., 2007). Carbon dioxide injection and methane  
598 production are simulated using TOUGH2; the link to the engineering components and  
599 an economic analysis is provided by GoldSim.



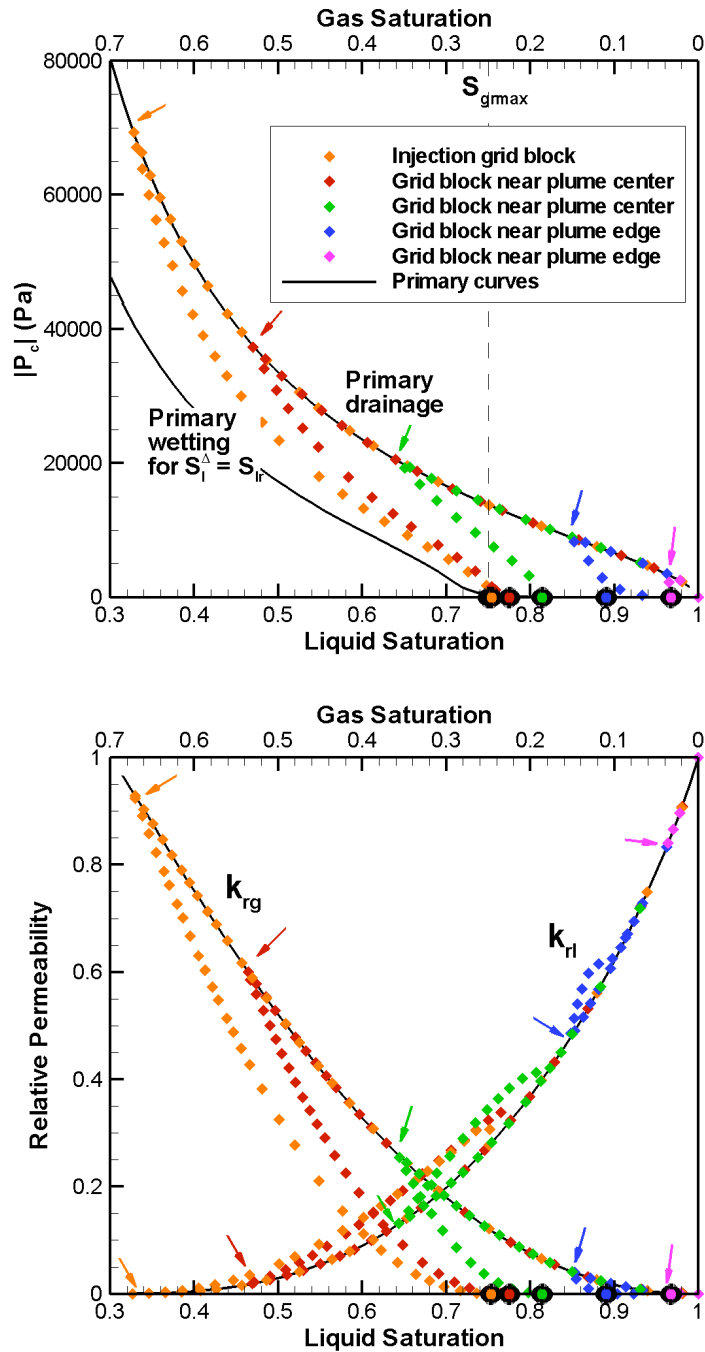
600

601 Figure 1. CO<sub>2</sub> plume evolution (from Doughty, 2007). The single black contour line

602 shows  $S_g = 0$ . The colored points identify the locations for which characteristic

603 curves are shown in Figure 2.

604



604

605 Figure 2. Hysteretic capillary pressure (top) and relative permeability (bottom) paths for

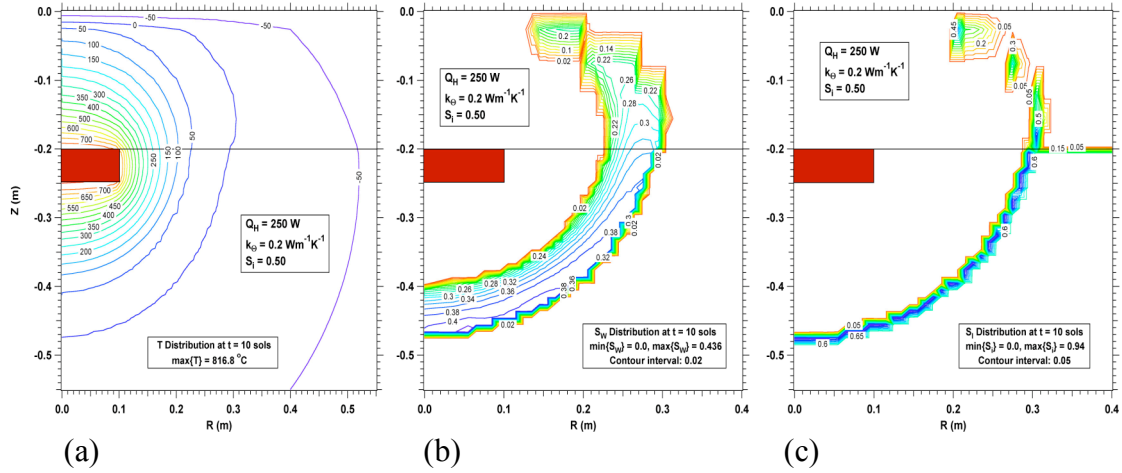
606 several grid blocks within the CO<sub>2</sub> plume (from Doughty, 2007). Grid-block

607 locations are shown in Figure 1. All paths start at  $S_l = 1$  on the primary drainage

608 curve.

609

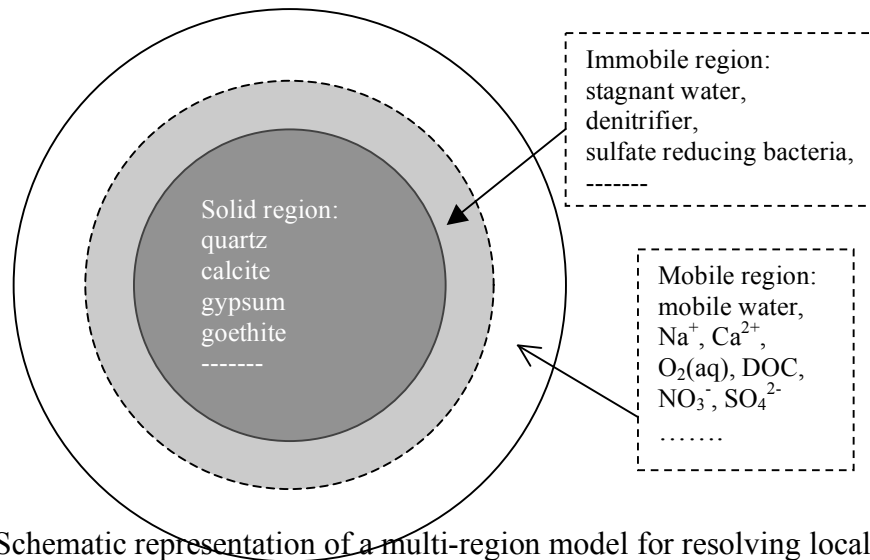




609  
610

611 Figure 3. Simulation of heat source buried in Martian permafrost (from Moridis and  
612 Pruess, 2006). (a) temperature, (b) water saturation, and (c) ice saturation after 10  
613 sols.

614



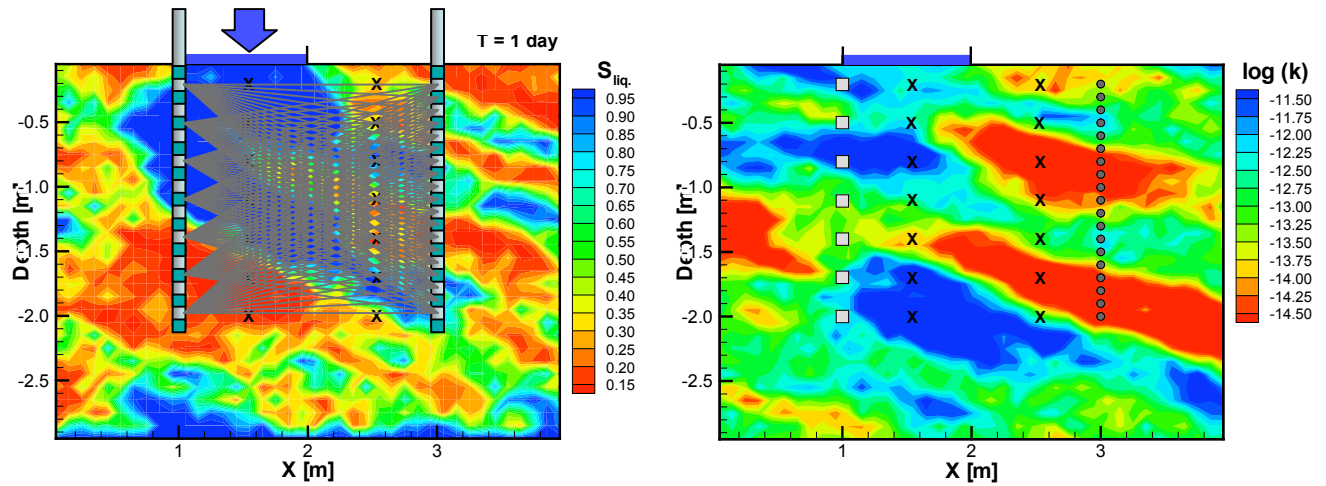
614

615 Figure 4. Schematic representation of a multi-region model for resolving local diffusive

616 transport (from Xu, 2007).

617

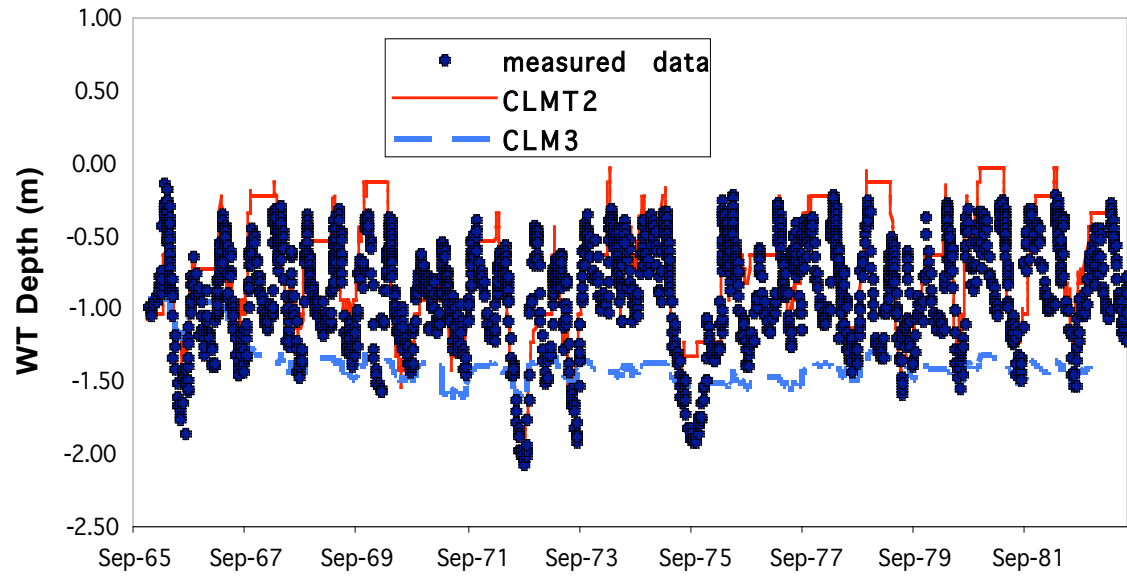




620  
621

622 Figure 6. Demonstration of joint hydrological-geophysical inversion approach for soil  
 623 structure identification (from Finsterle and Kowalsky, 2007). (a) Liquid saturation  
 624 distribution after one day of water release, locations of neutron probes in boreholes  
 625 (squares), and GPR straight-ray paths used for inversion; (b) site-specific  
 626 permeability field obtained by the joint estimation of geostatistical, hydrogeological,  
 627 and petrophysical parameters.

628



628

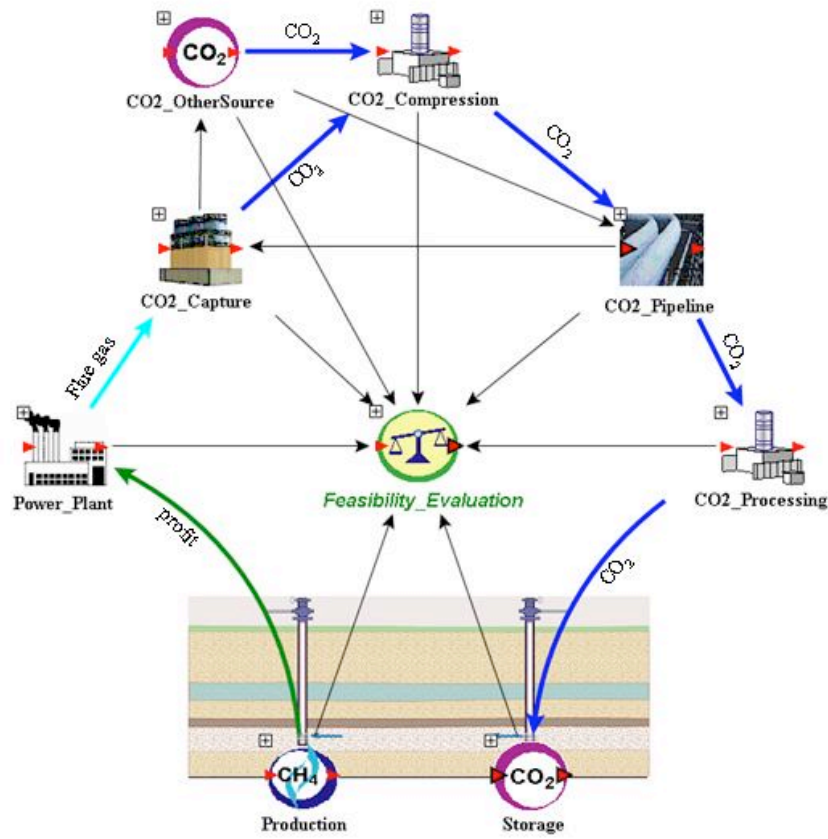
629

Figure 7. Comparison between observed and simulated daily water tables using

630

CLM3 and the coupled CLM3-TOUGH2 simulators (from Pan et al., 2007).

631



631

632 Figure 8. System-level model for the evaluation of carbon sequestration with enhanced

633 gas recovery (from Zhang et al., 2007). Carbon dioxide injection and methane

634 production are simulated using TOUGH2; the link to the engineering components and

635 an economic analysis is provided by GoldSim.

636